Top Catal (2017) 60:855–868
DOI 10.1007/s11244-017-0750-z

ORIGINAL PAPER

Non-Thermal Plasma-Assisted Catalytic Dry Reforming of Methane and Carbon Dioxide Over G-C_3N_4-Based Catalyst

Na Lu[1,2] · Xiaoding Bao[1] · Nan Jiang[1,2] · Kefeng Shang[1,2] · Jie Li[1,2] · Yan Wu[1,2]

Published online: 12 April 2017

Abstract In the present study, pure plasma and plasma-assisted catalytic activation of reforming of methane and carbon dioxide into syngas production were performed in a coaxial dielectric barrier discharge (DBD) plasma reactor at low temperature. For pure plasma, higher input power was favorable for the conversions of CH_4 and CO_2 but led to lower selectivities of syngas, while selectivities of syngas increased under lower flow rate of feed gases. A high CH_4/CO_2 ratio was more selective for C_2 hydrocarbon formation. Novel g-C_3N_4-based catalysts were prepared and filled in the discharge gap at low temperature. The cooperation effect of DBD plasma with g-C_3N_4 catalyst was achieved that contributed more to the activation of carbon dioxide than that of methane as well as the yield of CO for its low reduction potential. TiO_2/g-C_3N_4 with heterogeneous structure as packing the catalyst bulks into the discharge zone was capable of further improving the reforming of methane and carbon dioxide. TiO_2 mass ratio exhibited significant effect on dry reforming reactions and only TiO_2/g-C_3N_4 with 1% TiO_2 mass ratio presented enhanced hybrid effect than that of g-C_3N_4 catalyst.

Keywords Non-thermal plasma · Methane · Carbon dioxide · G-C_3N_4-based catalysts

✉ Na Lu
luna@dlut.edu.cn

[1] Key Laboratory of Industrial Ecology and Environmental Engineering (MOE), Dalian University of Technology, Dalian 116024, People's Republic of China

[2] School of Electrical Engineering, Dalian University of Technology, Dalian 116024, People's Republic of China

1 Introduction

Greenhouse gases, such as carbon dioxide (CO_2) and methane (CH_4), have been widely investigated through dry reforming of CH_4 and CO_2, producing syngas (CO and H_2) for source utilization and environmental protection [1–3]. The reforming of CO_2 and CH_4 has been reported via the following reaction [4–6].

$$CH_4 + CO_2 \rightarrow 2H_2 + 2CO,\ G_{298K} = 69\ kJ/mol$$

However, it is a thermodynamically unfavorable reaction that high operating temperature is required for the production of syngas from methane and carbon dioxide with low H_2/CO molar ratio. The traditional catalytic processes have been widely studied for the reforming of methane with carbon dioxide, while the problems of catalytic deactivation causing by coke deposition and active metals sintering at high operating temperature (above 937 K) usually restrain catalytic technology application [7]. Plasma technology can provide a large number of reactive species generated in the plasma field, including electrons, radicals, etc., which help to make the dry reforming reaction of methane. Non-thermal plasma has attracted increasing attention in recent years because of its low energy requirement [8–13]. Under non-thermal plasma, the reactant molecules such as CH_4 and CO_2 are readily captured by the high-energy electrons to give excited species and free radicals, which facilitate for further chemical reactions. A series of ionization, dissociation and excitation chemical process are initiated and the temperature of the reactants remains only at several 100 K [8].

Dielectric barrier discharge (DBD) plasma, as typical non-thermal plasma, possesses advantages of high electron temperature (1–10 eV) and electron density (10^{18}–10^{21} m^{-3}) [14–18], and has been widely investigated

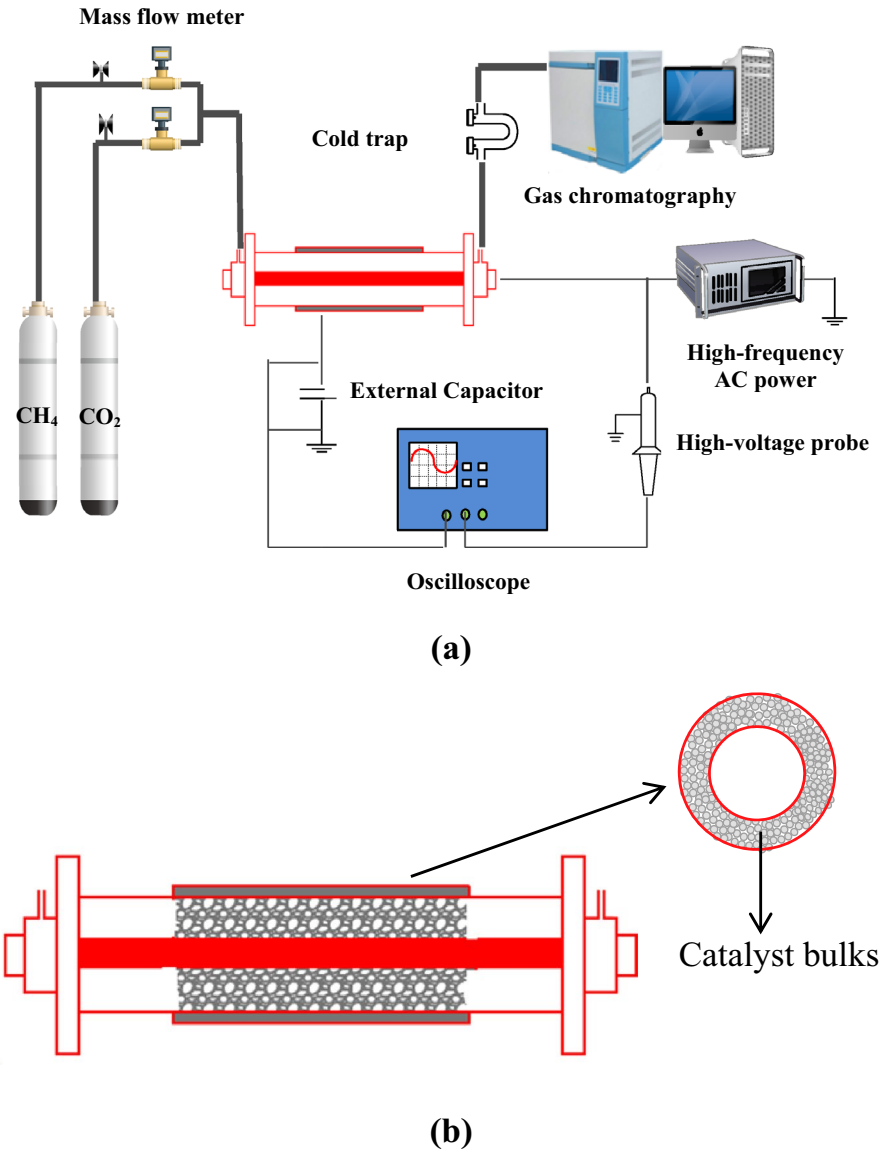

Fig. 1 Experimental system (**a**) and schematic diagram of reactor set-up (**b**)

to be effective for the dry reforming reaction at low temperature [19–23]. On the other hand, the dry reforming of methane under DBD plasma alone usually suffers from low conversion of reactants, poor selectivity of desired products and undesirable energy efficiency [12, 24–26]. The combination of a heterogeneous catalyst with DBD plasma has been reported to exhibit synergetic effect on improving the reaction performance both in conversion and selectivity [27–30]. Ni-based catalysts, Ni-based bimetallic oxides and La_2O_3/γ-Al_2O_3 catalyst have been extensively applied as catalysts in DBD reactor for the reforming of methane under atmosphere pressure [18, 29–34]. The catalyst placing in the plasma zone can affect discharge mode of DBD plasma that transfers from micro discharge to the combination of surface discharge and micro discharge [35, 36], and further the discharge stability can be destroyed in some cases [22, 30, 37]. The activation of catalyst in the discharge is found to be after the activation of the reactants [38]. However, effect of coke formation on catalysts in discharge zone is a problem facing by combination of DBD plasma and catalyst that leads to deactivation of the catalysts, and moreover the sintering of active metals is inevitable using metal-based catalyst, both of which cause reduction of carbon balance of plasma-catalysis much lower than 100% [25, 35, 39]. Furthermore, some studies have reported that combination of plasma with catalyst doesn't play a positive role in the reforming reaction of methane [14, 40]. Therefore, it is necessary to develop novel catalyst with improving catalytic performance in discharge zone for enhancing the dry reforming of methane.

Graphitic carbon nitride (g-C_3N_4) was firstly reported as a novel stable photocatalyst by Wang et al. in 2009 because

of its metal-free composition, non-toxicity and long-term stability [41], which is composed of carbon and nitrogen elements, possessing layered structure. Because of the band gap of approximately 2.7 eV [8, 42], g-C_3N_4 has been found to possess superior properties and exhibit efficient photocatalytic performance under visible light. Goettmann et al. reported that CO_2 could be activated by g-C_3N_4 [43] and Dong et al. also found that CO_2 could be reduced into CO [44]. Accordingly, g-C_3N_4 exhibits good application prospect in catalytic reduction of CO_2. Nevertheless, the catalytic efficiency of pure g-C_3N_4 is far from satisfaction due to its small surface area and short lifetimes of generated electrons and holes [45]. Coupling g-C_3N_4 and TiO_2 materials (g-C_3N_4 /TiO_2) is a promising strategy to improve the catalytic activity because of matched band gaps between g-C_3N_4 and TiO_2, which facilitates the separation of generated electrons from valence band (VB) of g-C_3N_4 (−1.12 eV vs. NHE) to conduction band (CB) of TiO_2 (−0.29 eV vs. NHE), as the VB edge potential of g-C_3N_4 is more negative than that of TiO_2. Under the powerful driving force causing by the differences in the CB edge potentials between g-C_3N_4 and TiO_2, the generated electron–hole pairs on the g-C_3N_4 surface are efficiently separated. TiO_2 acts as the acceptors of the generated electrons due to the matched band gaps between g-C_3N_4 and TiO_2. In DBD discharge zone, the high electron temperature is satisfactory to activate the g-C_3N_4/TiO_2 catalyst and it will be of important significance to exploring the feasibility of applying this novel catalyst for reforming of methane and carbon dioxide.

In this paper, CO_2 reforming of CH_4 to syngas by combination of DBD plasma with g-C_3N_4-based catalyst was studied under ambient conditions without extra heat to mitigate greenhouse emissions and reuse the carbon-hydrogen source. G-C_3N_4-based catalyst was firstly used as catalyst to convert methane and carbon dioxide because of its metal-free composition and good catalytic activity. The experimental conditions in the performed experiment and the effect of catalyst on the CO_2 reforming of CH_4 for syngas production are well investigated.

2 Experimental

2.1 Experimental System

The experimental system is shown in Fig. 1a. The non-thermal plasma-assisted catalytic experiments are performed in a coaxial DBD reactor that consists of a quartz tube with an inner diameter and thickness of 12 and 1.5 mm, respectively, as shown in Fig. 1b. A stainless tube with an inner diameter of 8 mm on the inside of the tube serves as high voltage electrode and the outer electrode is aluminum foil wrapping around the outer tube. The discharge length is

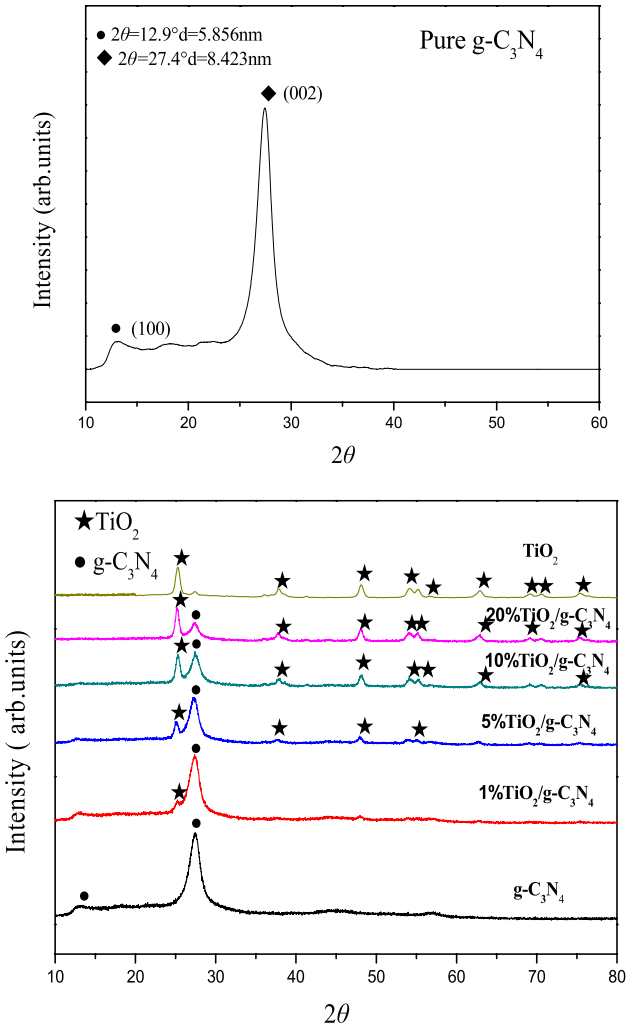

Fig. 2 XRD patterns of pure g-C_3N_4 and TiO_2/ g-C_3N_4

13 cm. DBD plasma is generated by an AC high-voltage generator (CTP-2000K) with a variable frequency of 4–12 kHz. A gas mixture of methane and carbon dioxide, controlled by mass flow controllers (MFC), flows to the DBD reactor. After reaction, on-line detection of the reaction mixture is performed on a gas chromatography (Shanghai Tianmei, GC7900) equipped with a thermal conductive detector (TCD) and a flame ionization detector (FID).

2.2 Preparation of G-C_3N_4-Based Catalysts

G-C_3N_4 was prepared by heating melamine powder (heating rate 5 °C/min) at 500 °C in a muffle furnace for 2 h and then heated at 520 °C for 2 h. After naturally cooling to room temperature, the yellow product was collected and milled into powder. TiO_2/g-C_3N_4 catalyst was prepared by mixing a certain amount of TiO_2 (P25) and melamine powder in absolute ethyl alcohol, stirring for 3 h, treating

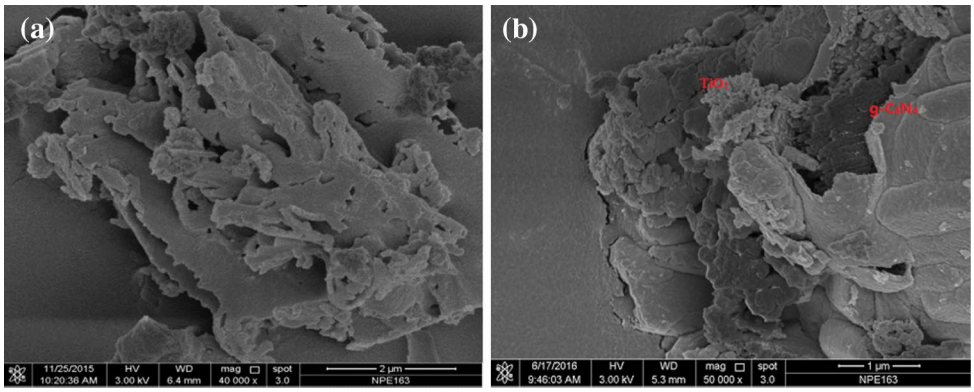

Fig. 3 SEM images of **a** g-C_3N_4 and **b** 1% TiO_2/g-C_3N_4

by ultrasound for 1 h, dried for 8 h, and finally heated at the same conditions of preparing g-C_3N_4. The product was milled into small pieces with average diameter of approximately 0.4–1.0 mm. TiO_2/g-C_3N_4 with different contents of TiO_2 was obtained. In the plasma-assisted catalytic experiments, the catalyst packed in the plasma zone was shown in Fig. 1b.

2.3 Characterization of Catalysts

The crystallinity characteristic of catalyst was determined using a X-ray diffractometer (Shimadzu, XD-3A) with Cu kα radiation at a scanning speed of 5 °C/min. The morphology of catalyst was observed on a NOVA Nano SEM 450 field-emission scanning electron microscope (FESEM). UV–Vis diffuse reflection spectra (UV-DRS) were recorded on UV–Vis spectrometer (UV-2450, Shimadzu) in the range of 200–800 nm using $BaSO_4$ as the reflectance standard. The X-ray photoelectron spectroscopy (XPS) measurement was performed using ESCALAB™ 250Xi XPS spectrometer equipped with Al Kα radiation in the fixed analyzer transmission mode. All peaks in XPS spectra have already been calibrated with C 1s peak at 284.6 eV. The Brunauer–Emmett–Teller (BET) of the catalyst was analyzed by nitrogen adsorption–desorption at 77 K in a Quantachrome AS-1 Fully automatic physical nitrogen adsorption instrument. The BET surface area was determined using adsorption data in a relative pressure (P/P_0) range of 0.05–0.3, and the Barrett–Joyner–Halenda (BJH) method was used to determine the pore-size distribution.

2.4 Analytical Method

In the present work, the reactants and products were analyzed by an on-line gas chromatography. The CH_4 and CO_2 conversions, products selectivities, yields of products, and carbon balance are defined as follows:

$$C_{CO_2}(\%) = \frac{CO_2 \text{ converted (mol/s)}}{CO_2 \text{ input (mol/s)}} \times 100$$

$$C_{CH_4}(\%) = \frac{CH_4 \text{ converted (mol/s)}}{CH_4 \text{ input (mol/s)}} \times 100$$

$$S_{CO}(\%) = \frac{CO \text{ produced (mol/s)}}{CO_2 \text{ converted (mol/s)} + CH_4 \text{ converted (mol/s)}} \times 100$$

$$S_{H_2}(\%) = \frac{H_2 \text{ produced (mol/s)}}{2 \times CH_4 \text{ converted (mol/s)}} \times 100$$

$$S_{C_2H_6}(\%) = \frac{C_2H_6 \text{ produced} \times 2 \text{ (mol/s)}}{CO_2 \text{ converted (mol/s)} + CH_4 \text{ converted (mol/s)}} \times 100$$

$$Y_{CO}(\%) = \frac{CO \text{ produced (mol/s)}}{CO_2 \text{ input (mol/s)} + CH_4 \text{ input (mol/s)}} \times 100$$

$$Y_{H_2}(\%) = \frac{H_2 \text{ produced (mol/s)}}{2 \times CH_4 \text{ input (mol/s)}} \times 100$$

$$Y_{C_2H_6}(\%) = \frac{C_2H_6 \text{ produced (mol/s)} \times 2}{CO_2 \text{ input (mol/s)} + CH_4 \text{ input (mol/s)}} \times 100$$

$$S_{CH_4 \text{ to } CO_2}(\%) = \frac{CO \text{ produced (mol/s)} - CO_2 \text{ converted (mol/s)}}{CH_4 \text{ converted (mol/s)}} \times 100$$

$$B_{carbon}(\%) = \frac{CO \text{ produced (mol/s)} + CO_2 \text{ produced (mol/s)} + C_xH_y \text{ produced (mol/s)} \times x}{CO \text{ input (mol/s)} + CH \text{ input (mol/s)}} \times 100$$

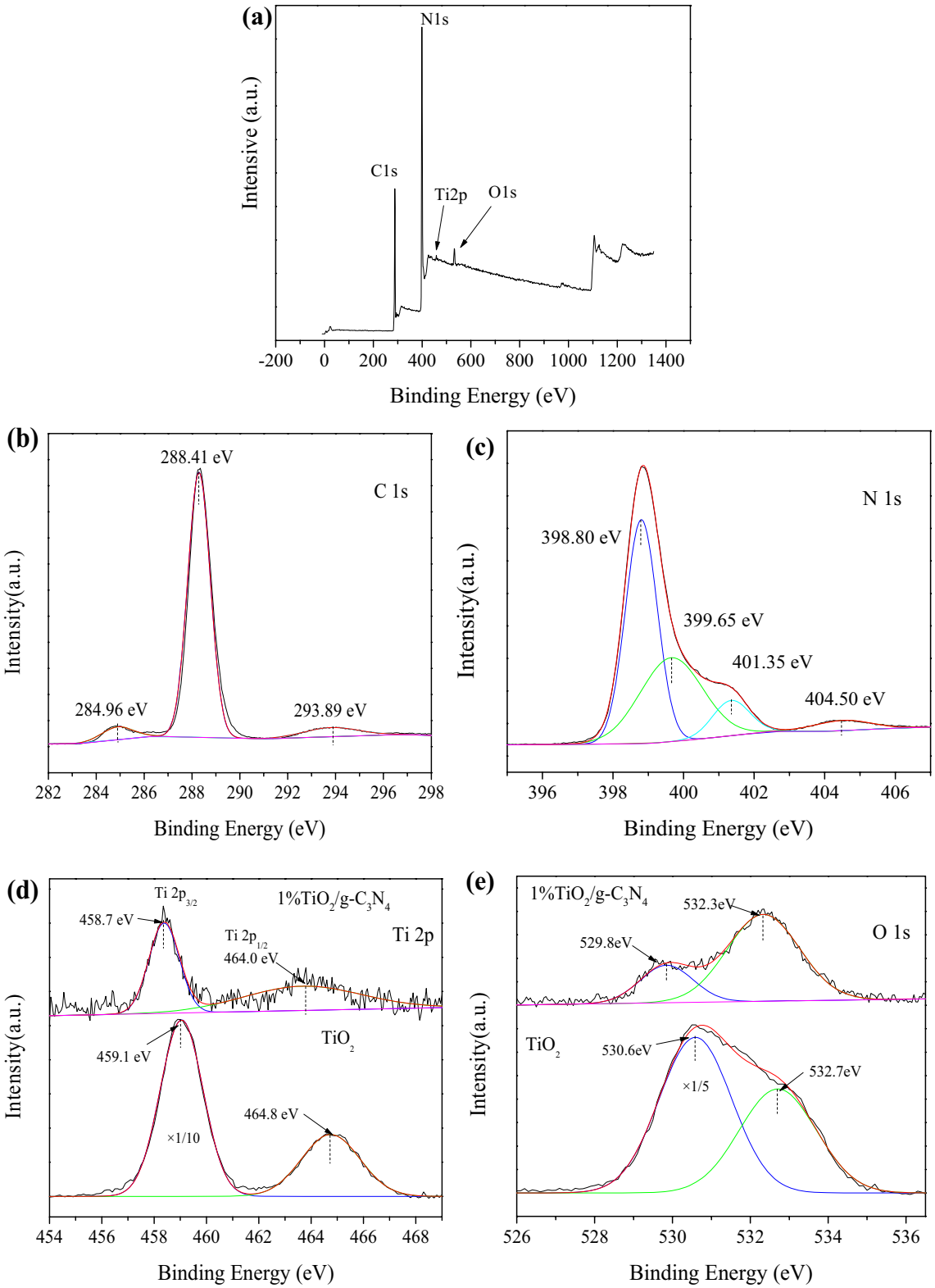

Fig. 4 XPS of **a** survey spectrum, **b** C 1s and **c** N 1s for 1% TiO_2/g-C_3N_4, **d** Ti 2p and **e** O 1s for 1% TiO_2/g-C_3N_4 and pure TiO_2

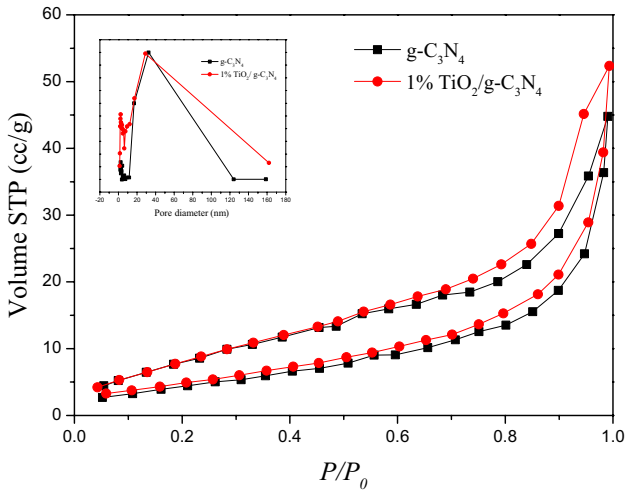

Fig. 5 Nitrogen adsorption–desorption isotherms and corresponding pore size distribution (*inset*) of the g-C_3N_4 and 1% TiO_2/g-C_3N_4

Specific energy density (*SED*) and energy utilization efficiency (*E*) are defined as:

$$SED\ (\mathrm{kJ/L}) = \frac{\text{Discharge power (kW)}}{\mathrm{CO_2}\ \text{flow rate (L/s)} + \mathrm{CH_4}\ \text{flow rate (L/s)}}$$

$$E(\mathrm{mol/kJ}) = \frac{\mathrm{CO_2}\ \text{converted (mol/s)} + \mathrm{CH_4}\ \text{converted (mol/s)}}{\text{Power input (kW)}}$$

3 Results and Discussion

3.1 Characterization of Catalysts

The phase structures of the prepared catalysts are determined by XRD analysis. XRD patterns of pure g-C_3N_4, and TiO_2/g-C_3N_4 prepared at different mass rations of g-C_3N_4 and TiO_2 are illustrated in Fig. 2. The pure g-C_3N_4 shows two characteristic diffraction peaks at 13.1° and 27.4° (JCPDS No. 87-1526). The minor peak of (100) at 13.1° and the stronger peak of (002) at 27.4° correspond to the inter-layer structural packing [46] and the interplanar graphitic stacking of aromatic system [47], respectively. The phases of TiO_2 are observed in the TiO_2/g-C_3N_4 samples. With the increase of the mass ratio of TiO_2 in the TiO_2/g-C_3N_4, the intensity of the diffraction peak of (101) at 25.2°, assigning to anatase phase (JCPDS No. 21-1272) of TiO_2, becomes stronger, while the

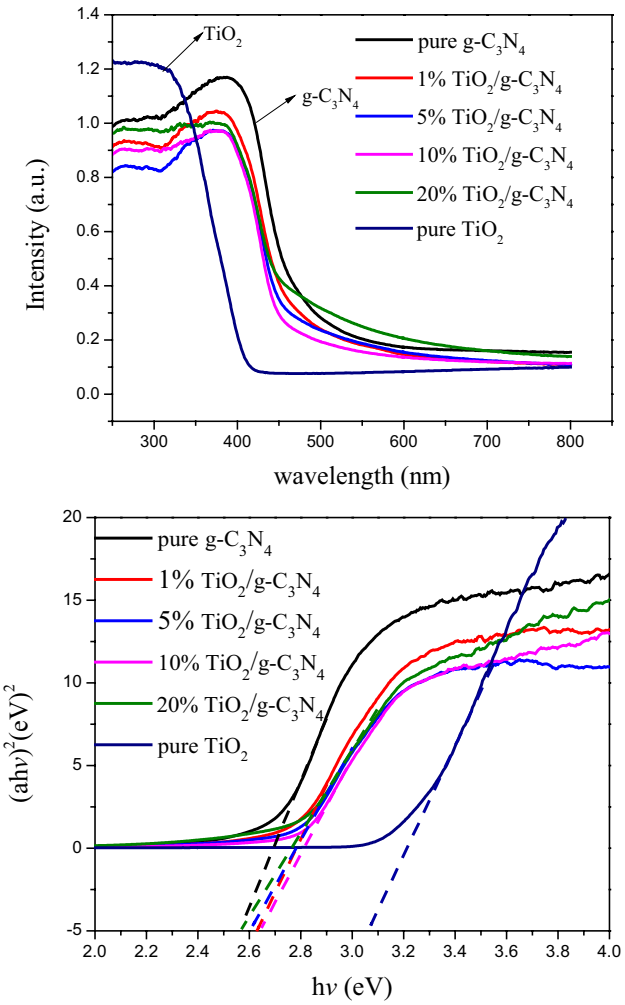

Fig. 6 UV–vis absorption spectra of pure g-C_3N_4, pure TiO_2, and TiO_2/g-C_3N_4 composite with different ratios

diffraction peak intensity at 27.6° of g-C_3N_4 becomes weaker. In addition, the peak positions for all TiO_2/g-C_3N_4 samples are observed to keep unchanged, indicating that TiO_2 probably deposits on the surface of g-C_3N_4.

SEM imaging is performed to observe the morphologies of g-C_3N_4 and TiO_2/g-C_3N_4. From the point of the entire field of vision (Fig. 3a), it fills with large number of continuous lamellar g-C_3N_4 with 2D lamellar structure. As shown in Fig. 3b, after mixing TiO_2 (1%) with g-C_3N_4, TiO_2 is loaded on the surface of g-C_3N_4, which is benefited for the formation of heterojunction between g-C_3N_4 and TiO_2. The surface

Table 1 Specific surface area of the as-prepared samples with the different amount of TiO_2 in TiO_2/g-C_3N_4 composite

Sample	g-C_3N_4	1% TiO_2/g-C_3N_4	5% TiO_2/g-C_3N_4	10% TiO_2/g-C_3N_4	20% TiO_2/g-C_3N_4
Specific surface area (m^2/g)	14.1	18.2	22.1	33.5	21.5
Pore volume (cc/g × 10^{-3})	0.0072	0.0087	0.0108	0.017	0.011

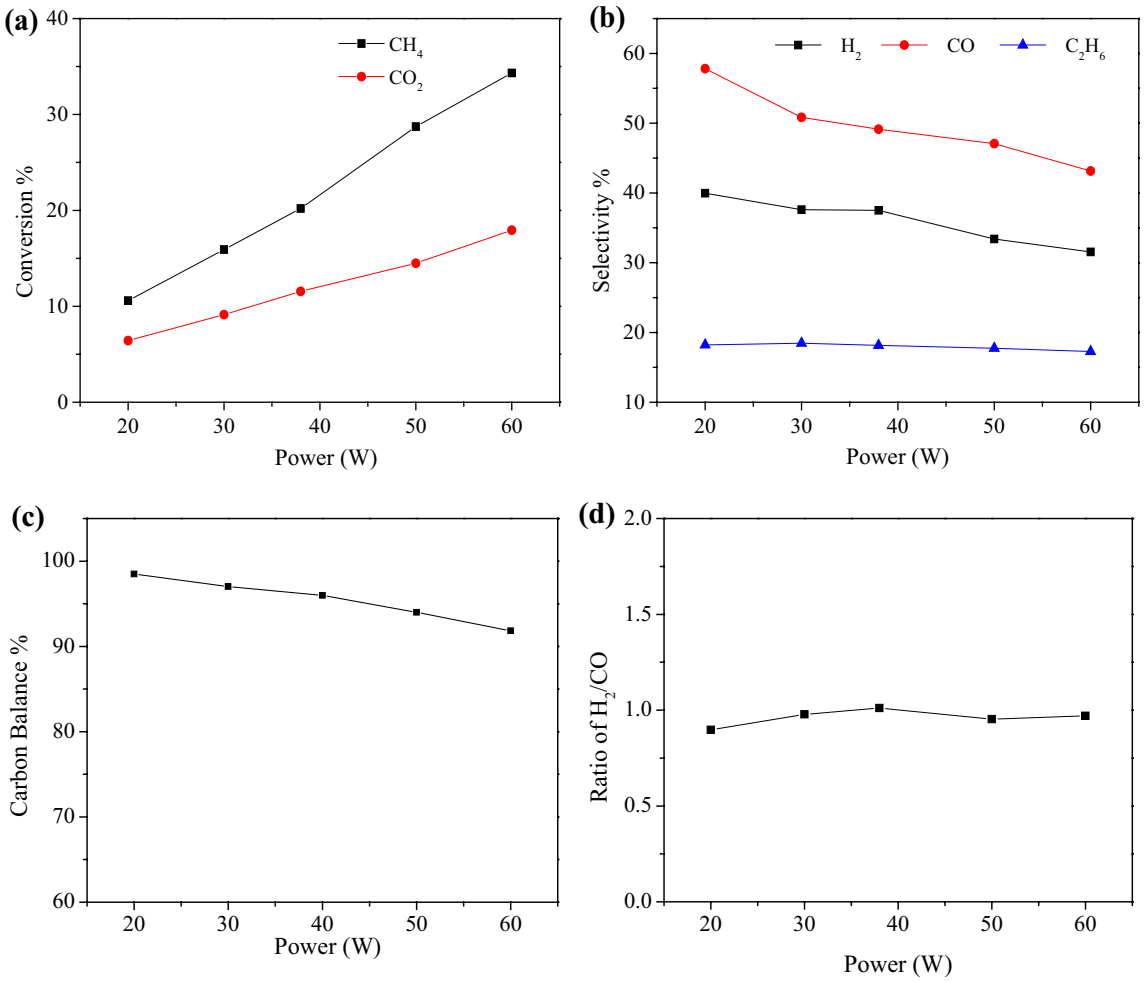

Fig. 7 Effect of discharge power on the performance of dry reforming reaction: **a** conversion of reactants; **b** selectivity of main products; **c** carbon balance; **d** ratio of H_2/CO ($CH_4/CO_2 = 1{:}1$, feed flow rate 50 mL/min)

of TiO_2 is rough and porous, possibly being caused by the agglomeration of TiO_2 to some extent due to the calcination treatment.

The XPS survey spectrum of TiO_2/g-C_3N_4 sample is shown in Fig. 4a, in which C 1s, N 1s, Ti 2p and O 1s can be observed. The weak peaks of Ti and O are the results of low amount of TiO_2 in the TiO_2/g-C_3N_4 composite. Figure 4b shows the spectrum of C 1s for TiO_2/g-C_3N_4 sample. The peaks at about 284.96, 288.41 and 293.89 eV correspond to C–C, C–N–C and C–$(N)_3$ groups in the g-C_3N_4, respectively [48]. Figure 4c shows the spectrum of N 1s for TiO_2/g-C_3N_4 that displays four peaks, ascribable to sp_2 hybridized nitrogen (C=N–C) at about 398.8 eV, tertiary N in N–$(C)_3$ at about 399.65 eV, N atoms in amino moieties at about 401.35 eV [49], and weak peak located at 404.2 eV which is due to the charging effects or positive charge localization in the heterocycles [50]. Figure 4d presents the Ti 2p spectra of TiO_2/g-C_3N_4 and pure TiO_2. Two peaks for Ti $2p_{3/2}$ and Ti $2p_{1/2}$ of pure TiO_2 located at 459.1 and 464.8 eV, and the peaks at 458.7 and 464.0 eV correspond to Ti $2p_{3/2}$ and Ti $2p_{1/2}$ of TiO_2/g-C_3N_4, respectively. Comparison of O 1s spectra of TiO_2/g-C_3N_4 and pure TiO_2 is shown in Fig. 4e. The blinding energies of 530.6 eV and 532.7 eV for pure TiO_2 can be ascribed to Ti-O bond and O-H bond, respectively [48]. Compared with pure TiO_2, O 1s spectrum of TiO_2/g-C_3N_4 shows the negative shift with an order of 0.8 eV, and the same shift of Ti 2p in Fig. 4b is also observed, which indicates that chemically bound interfaces may be formed between g-C_3N_4 and TiO_2 phase.

The nitrogen adsorption–desorption isotherms of g-C_3N_4 and 1% TiO_2/g-C_3N_4 were present in Fig. 5. It can be seen that both samples have the isotherms type of H4 according to the IUPAC (International Union of Pure and

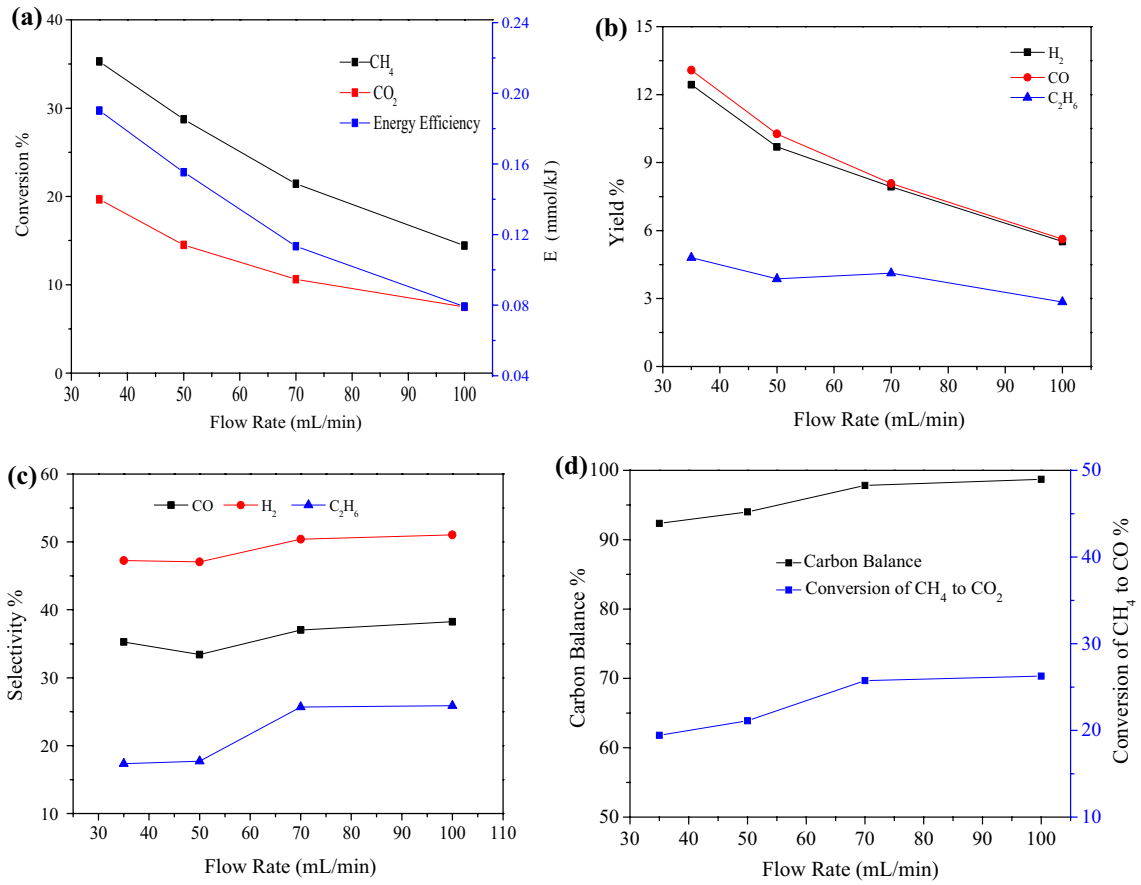

Fig. 8 Effect of total flow rate on the performance of plasma dry reforming reaction: **a** conversion of reactants and energy efficiency; **b** yield of main products; **c** selectivity of main products; **d** carbon balance ($CH_4/CO_2 = 1:1$, discharge power 50 W)

Applied Chemistry) classification, which indicates irregular pore structure and micropore and mesopore both exist in the samples [51]. The graph insert in Fig. 5 shows the pore-size distributions of g-C_3N_4 and 1% TiO_2/g-C_3N_4, which are broad and the samples are mainly composed by mesopore. Specific surface area (S_{BET}) of the as-prepared samples with different amount of TiO_2 in g-C_3N_4 was shown in Table 1. The S_{BET} increases with the increasing amount of TiO_2 except 20%TiO_2/g-C_3N_4, which is possibly attributed to the sintering caused by calcine process.

The optical absorption properties of TiO_2, g-C_3N_4 and as-prepared TiO_2/g-C_3N_4 samples are investigated by UV-DRS analysis, as shown in Fig. 6. The absorption edge for TiO_2 is under 400 nm, only having a response to UV light. The g-C_3N_4 exhibits a wider photo-absorption till visible light, the main absorption edge of which occurs at approximately 500 nm due to its wide band gap of 2.57 eV. For TiO_2/g-C_3N_4 samples, a certain extent red-shift of the absorption edge to visible region and a certain extent blue-shift of the absorption edge to UV region are observed as compared to pure TiO_2 and pure g-C_3N_4, respectively, indicating the band gap of g-C_3N_4 becomes narrower when combing it with TiO_2. In the plasma zone, the catalyst is expected to be excited by the active species in the plasma with energy higher than 2.7 eV, exhibiting catalytic performance on reforming of methane efficiently.

3.2 Effect of Discharge Power on the Plasma Dry Reforming Reaction

Under non-thermal plasma, the discharge power determines the strength of the internal electric field and the electron energy, which is important for inelastic collisions between energetic electrons and reactant molecules. In the present work, the conversions of CO_2 and CH_4 were found to increase from 6% and 11% to 18% and 34%, respectively, with the discharge power increasing from 20 to 60 W. High level of discharge power provides more energy for the formation of active species, such as electrons, $^{\cdot}OH$, and $O^{\cdot}$, which are likely to attack CH_4 and CO_2, leading to enhanced conversions of reactants. It is also found that the conversion of CH_4 is

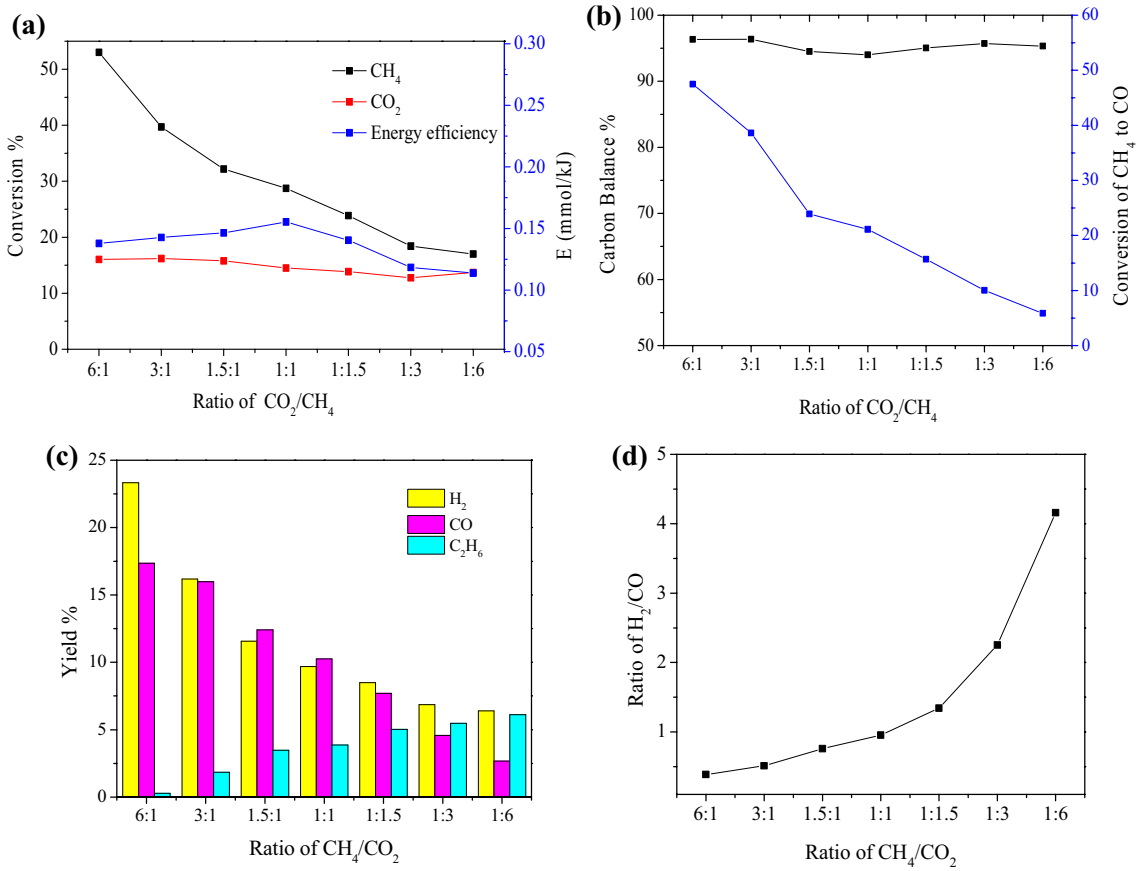

Fig. 9 Effect of CO_2/CH_4 ratio on the performance of dry reforming reaction: **a** conversion of reactants and energy efficiency; **b** carbon balance and the ratio of CH_4 convert to CO; **c** yield of main products; **d** ratio of H_2/CO (feed flow rate 50 m L/min, discharge power 50 W)

always higher than that of CO_2 as shown in Fig. 7a. Similar result is also reported in [30]. With the increase of discharge power, the balance between the dehydrogenation rates of CH_x (x = 1–4) radicals and the dissociation rate of active CO_2 species can be deteriorated causing by the excess energy. The result of the breaking of the balance favors for the reaction between H and O but is disadvantageous for the generation of CO from C and O atoms [52]. The selectivities of CO and H_2 decreased with the increase of discharge power (Fig. 7b), indicating the coke formation at higher energy level, the results of which consist with the conversions of CO_2 and CH_4. Gaseous hydrocarbon, C_2H_6, existing in the products, is possibly formed by the complex reaction between two CH_3 radicals. In Fig. 5b, the selectivity of C_2H_6 hardly changed with the increasing discharge power, suggesting that C_2H_6 formation was not affected by the discharge power. The carbon balance was found to decrease with the increase of discharge power (Fig. 7c), further supporting the facts of coke formation at higher energy level. As shown in Fig. 7d, discharge power exhibited less effect on the H_2/CO ratio, which indicated the consistent changes of H_2 formation and CO formation was not affected with the increase of discharge power.

3.3 Effect of Total Flow Rate on the Plasma Dry Reforming Reaction

The total flow rate of feed determines the residence time of the reactants in the discharge zone and its effect on the plasma dry reforming reaction is shown in Fig. 8. For a constant input power, the conversions of CH_4 and CO_2 decreased from 35.3% and 19.7% to 14.4% and 7.5% (Fig. 8a), respectively, and the yields of CO and H_2 both decreased by approximately 56% (Fig. 8b), but the selectivities of CO and H_2 changed slightly (Fig. 8c), with the increase of total flow rate from 35 to 100 mL/min. The total flow rate also influenced the formation of the hydrocarbon byproduct, C_2H_6, the yield of which decreased by 42%, while the selectivity of it increased obviously. It is apparent that increasing the total flow rate benefits the conversion of CH_4 to hydrocarbon byproduct. As shown

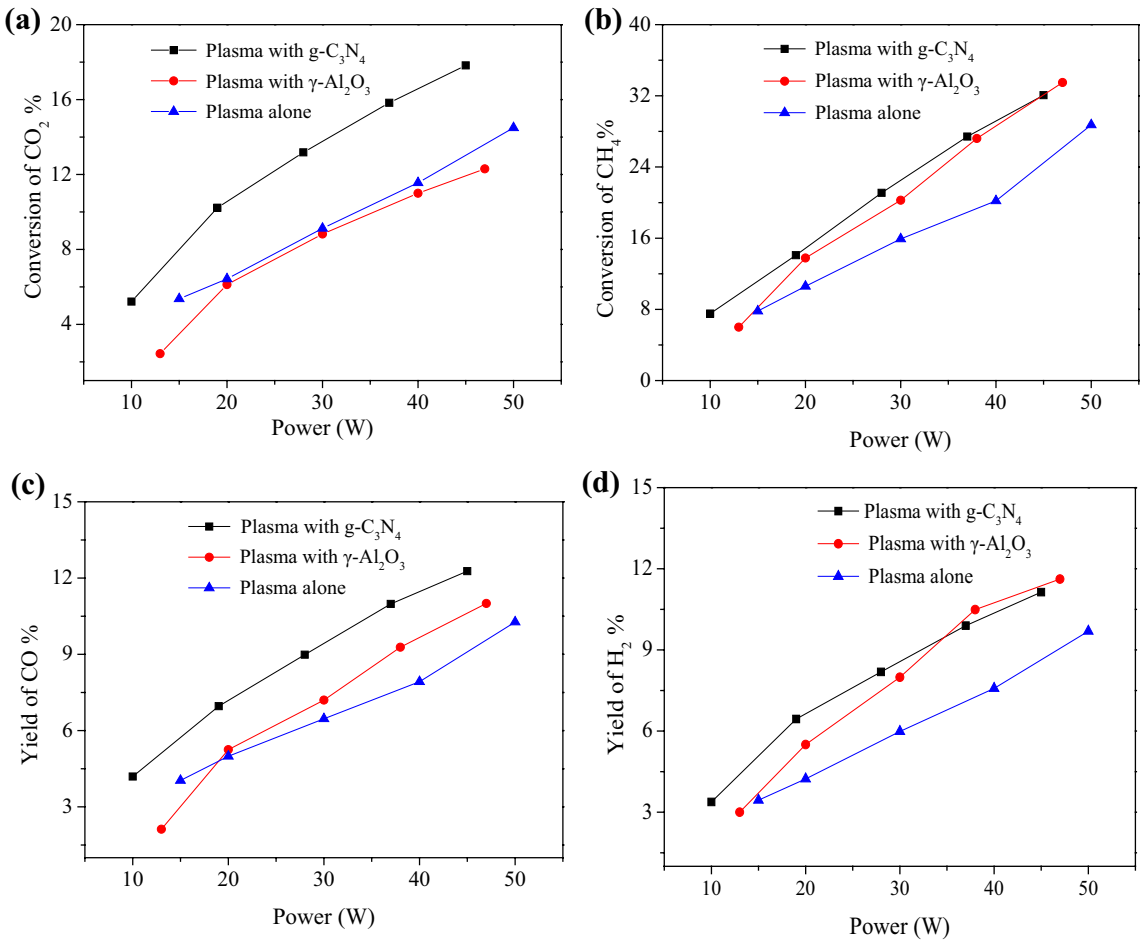

Fig. 10 Effect of packing g-C_3N_4 catalyst and γ-Al_2O_3 in plasma discharge area on the performance of plasma dry reforming reactions: **a** conversion of CH_4; **b** conversion of CO_2; **c** yield of CO; **d** yield of H_2. ($CH_4/CO_2 = 1{:}1$, feed flow rate 50 mL/min)

in Fig. 6d, the carbon balance as well as conversion of CH_4 to CO increased with the total flow rate, because increase of the flow rate would reduce the collision chance among CH_x active species, and thus more CH_4 was converted to low-carbon hydrocarbon compounds such as C_2H_6 and CO instead of long chain hydrocarbons. Energy efficiency is found to decrease when increasing the total flow rate, which is caused by the reduction of residence time of reactants and active species in plasma zone. On the consideration of the effect of the total flow rate on the dry reforming reaction, the optimal flow rate of 50 mL/min is selected in the following experiments.

3.4 Effect of CO_2/CH_4 Ratio on the Plasma Dry Reforming Reaction

Effect of reagent composition on the plasma dry reforming reaction is performed by varying the CO_2/CH_4 ratios from 6/1 to 1/6 at a constant total flow rate (50 mL/min) and a constant discharge power (50 W). The results are shown in Fig. 9. With the increase of molar ratio of CH_4 to CO_2, the conversion of CH_4 was always higher than that of CO_2. However, the CO_2/CH_4 ratio had greater influence on the conversion of CH_4 which decreased from 53% to 17% obviously but the conversion of CO_2 changed slightly. As shown in Fig. 9b, the yields of H_2 and CO both decreased with the increase of molar ratio of CH_4 to CO_2 while the yield of C_2H_6 increased. Figure 9c further exhibited the fact that increasing the amount of CH_4 in the feed gas would restrain its conversion to CO. These experimental results can be explained by the possible reactions involving active methane species, the amount of which increase with the CH_4 molar, and thus more active methane species involve in recombination reaction than methane oxidation to form CO, generating more hydrocarbons [18, 30]. In the present studied range of CO_2/CH_4 ratios, the carbon balance kept at approximately 95% while the ratio of H_2/CO increased significantly with the increasing CH_4/CO_2 ratio (Fig. 9d). This result further

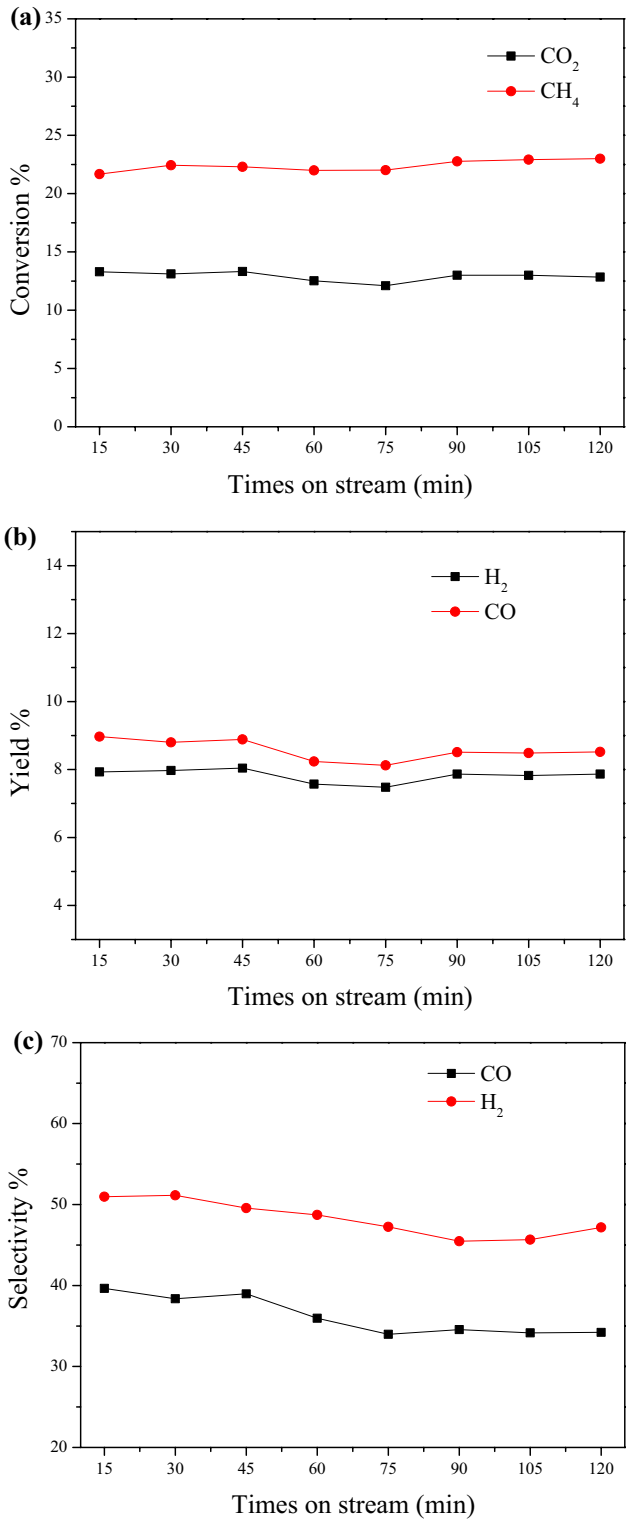

Fig. 11 Stability of g-C_3N_4 catalyst with the increase of reaction time: **a** conversion, **b** yield and **c** selectivity

confirms that increasing CH_4/CO_2 ratio leads to less oxygen, favoring for the production of hydrocarbon accompanying by carbon deposition.

3.5 Plasma-Catalyst Association

Combination of non-thermal plasma with catalysts has been widely investigated in dry reforming reactions aiming at improving the conversion and selectivity. For non-thermal plasma, most of the electrical energies provided by the input power are consumed for energetic electrons production, which play key role in plasma-alone assisted dry reforming by way of reacting with reactants molecules to generate excited species. With the presence of catalyst bulks in the discharge gap, surface discharge may occur on the surface of the catalyst and the catalyst can trap energetic electrons in the active particles. Accordingly, effect of catalyst on the discharge process other than catalytic activity should be under consideration to clarify the plasma-catalyst association for dry reforming reaction.

In the present work, samples of g-C_3N_4 and γ-Al_2O_3 with the same particle size are placed in the discharge zone, respectively. The γ-Al_2O_3 has no catalytic activity and here helps to explore how the drying reforming reaction is influenced by the sample packing that might cause the discharge process change. Effect of input power on the conversions of reactants and the yields of CO and H_2 over the catalyst samples placed at the DBD reactor is shown in Fig. 10. As γ-Al_2O_3 was packed in the discharge zone, the conversion of CH_4 as well as yield of H_2 increased to some extent, while the conversion of CO_2 changed slightly and the increase in yield of CO was lower than that of H_2. The results exhibit the fact that the change of discharge mode causing by γ-Al_2O_3 packing would affect the dry reforming reaction. After γ-Al_2O_3 packing, the discharge mode transfers from filament discharge to the combination of filament discharge and surface discharge. Polarization field is formed on the surface of γ-Al_2O_3 particles, making the electric field intensity in local area strengthen. The reason of the enhancements of the conversion of CH_4 and yield of H_2 is due to lower dissociation energy of CH_4 than that of CO_2. The followings are the main reactions happened in the discharge zone.

$$e + CO_2 \rightarrow CO + O + e \quad (1)$$

$$e + CH_4 \rightarrow CH_3 + H + e \quad (2)$$

$$e + CH_3 \rightarrow CH_2 + H + e \quad (3)$$

$$e + CH_2 \rightarrow CH + H + e \quad (4)$$

$$e + CH \rightarrow C + H + e \quad (5)$$

$$C + O \rightarrow CO \quad (6)$$

In case of g-C_3N_4, the conversions of CH_4 and CO_2 increased and the yields of H_2 and CO were all higher than those obtained in plasma-alone system. As a novel

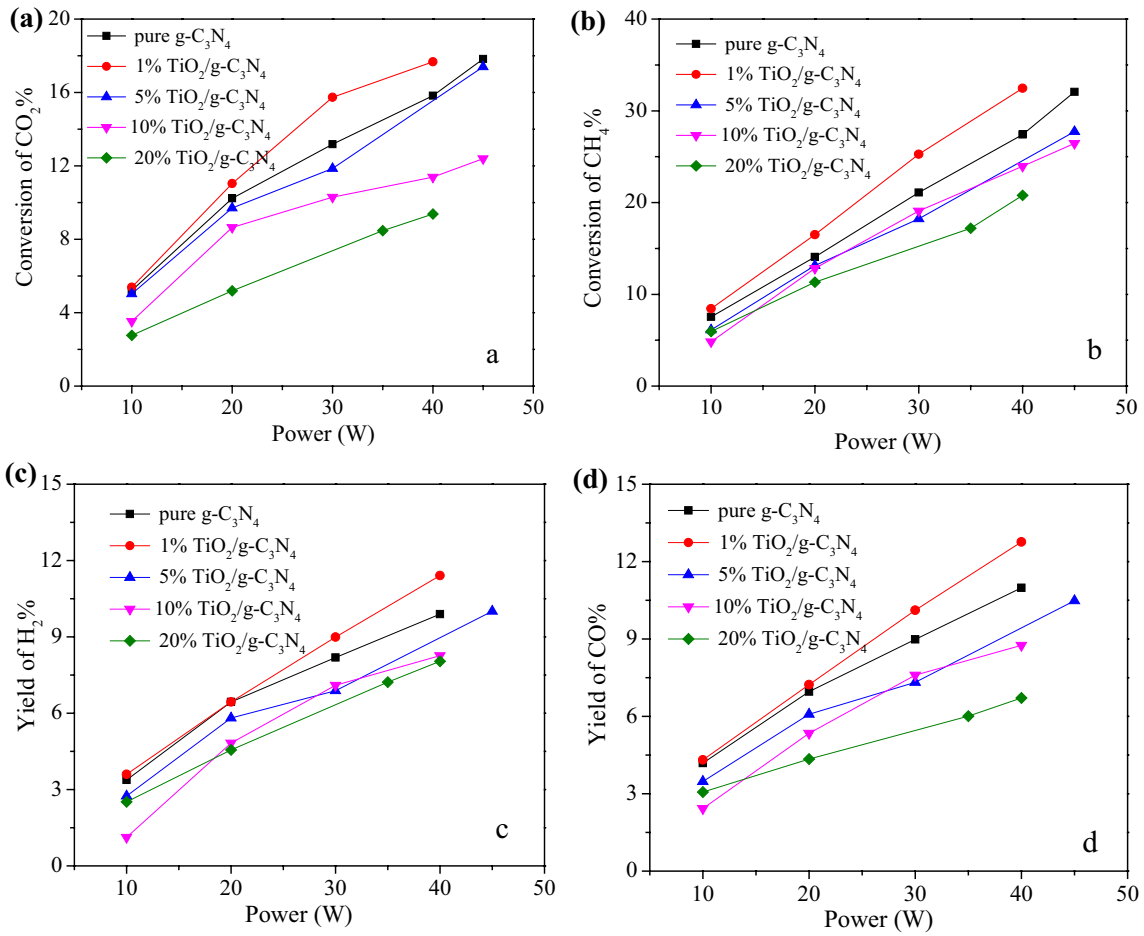

Fig. 12 Effect of TiO_2/g-C_3N_4 composite packing in discharge area with different TiO_2 mass ratios on the performance of dry reforming reaction: **a, b** conversions of reactants; **c, d** yield of products. ($CH_4/CO_2 = 1:1$, feed flow rate 50 mL/min)

metal-free catalyst, it can be excited by DBD plasma because its narrow band gap (2.7 eV), and moreover, the generated electrons have a strong reducing ability because of extremely negative position (−1.35 vs. NHE) of the g-C_3N_4 conduction band, which is expected to favor the conversion of CO_2 in the dry reforming reaction. Furthermore, the results are also higher than those using γ-Al_2O_3 particles in plasma zone. The cooperation effect of DBD plasma with g-C_3N_4 catalyst is verified. Compared with plasma-alone, stronger externally applied electric field as well as stronger micro- and surface discharges are formed as packing g-C_3N_4 catalyst into DBD plasma zone. More excited species are adsorbed on the surface of the catalyst and favors the conversion of the reactants comparing, achieving desired products [34].

The stability of g-C_3N_4 prepared in this study was tested under the conditions of discharge power 30 W, flow rate of feed gas 50 mL/min and molar ratio of CH_4/CO_2 1:1. The product was detected every 15 min by the on-line detection and the results was shown in Fig. 11. After 120 min treatment, the as-prepared catalyst performed a favorable stability in the conversion of CH_4 and CO_2.The yield and selectivity of main products of H_2 and CO slightly decrease after 45 min reaction which may be attributed to the carbon formation during the collision of high energy electrons and CH_4.

Pure g-C_3N_4 usually suffers from small surface area and short lifetimes of generated electrons and holes. Approach of constructing heterogeneous structure by coupling g-C_3N_4 and TiO_2 materials is a promising strategy to improve the charge separation efficiency. Accordingly, TiO_2/g-C_3N_4 catalysts with different TiO_2 mass ratio were prepared in the present work and the catalytic activity towards dry reforming reaction is explored. As shown in Fig. 12, the TiO_2 mass ratio exhibited significant effect on dry reforming reactions. Only TiO_2/g-C_3N_4 with 1% TiO_2 mass ratio presented a hybrid effect as packing the catalyst bulks into the discharge zone. The efficient separation of electrons and holes occurred when mixing TiO_2 (1%) with g-C_3N_4. However, further increasing mass ratio of TiO_2 restrained

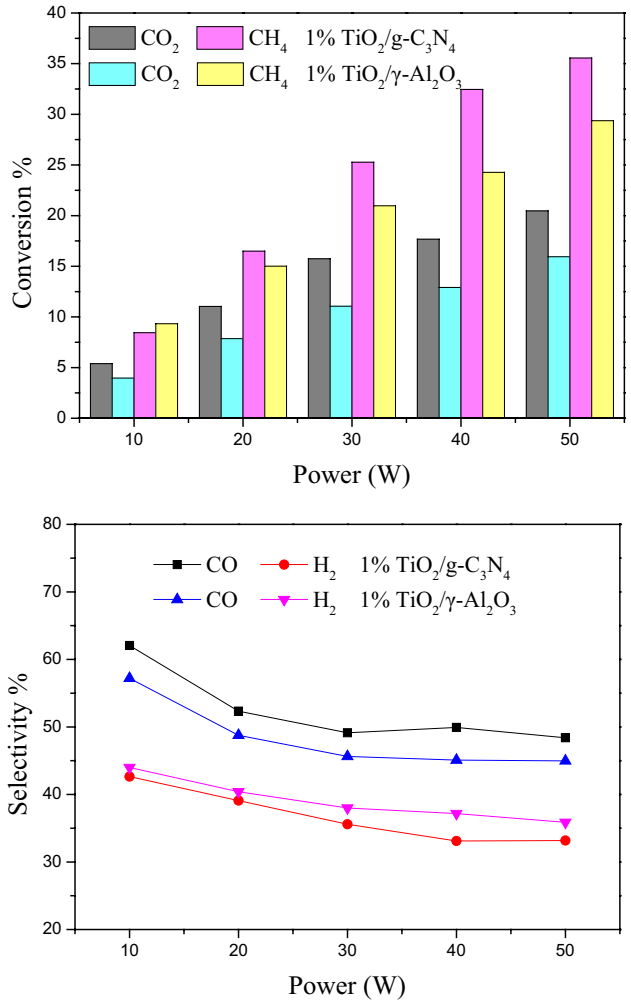

Fig. 13 Conversions of CH_4 and CO_2, and selectivities of CO and H_2 as the DBD reactor packing with 1% TiO_2/g-C_3N_4 and 1% TiO_2/γ-Al_2O_3 catalysts, respectively

the conversions of feed gases and also the yields of CO and H_2. The reasons can be explained by the higher dispersion of TiO_2 on the surface of g-C_3N_4 with further increasing the mass ratio of TiO_2, which could adsorb more high energy electrons and thus reduce the reaction probability between high energy electrons and g-C_3N_4. In the present work, the electron energy might not be higher enough to excite TiO_2, whose band gap is 3.1 eV, and thus excitation of g-C_3N_4 is expected to play significant role in the plasma-assisted catalytic reaction and 1% of TiO_2 is believed to contribute to improve separation of electrons and holes generated on g-C_3N_4. Control experiment was further carried out with 1% TiO_2/γ-Al_2O_3, which prepared in same synthesis procedure of 1% TiO_2/g-C_3N_4, and the results are shown in Fig. 13. As the discharge area packing with 1% TiO_2/g-C_3N_4 and 1% TiO_2/γ-Al_2O_3 catalysts, respectively, with the increasing of discharge power, conversions of CO_2 and CH_4 increase while the selectivities of main products decrease, which is in accordance with aforementioned result. Comparing the catalytic activity of TiO_2/g-C_3N_4 with TiO_2/γ-Al_2O_3 combining with DBD plasma, TiO_2/g-C_3N_4 exhibits better performance in both CO_2 and CH_4 conversion and the selectivity of CO, while the selectivity of H_2 is slightly lower than that using TiO_2/γ-Al_2O_3 catalyst. The experimental result further proves the good catalytic activity of TiO_2/g-C_3N_4 composite in conversion of CO_2 and CH_4 and enhancing CO selectivity. However, the detailed mechanism of DBD plasma- g-C_3N_4-based catalysis has not been fully understood yet. The appropriate optimization of the DBD plasma-assisted g-C_3N_4-based catalytic system is needed to be further studied.

4 Conclusion

Dry reforming of methane and carbon dioxide under pure plasma and synthetic action of plasma-assisted g-C_3N_4-based catalysis was investigated in DBD reactor. In pure plasma process, input power, total flow rate of feed gas and CH_4/CO_2 ratio affected the reaction. High input power and low total flow rate favored for increasing the conversions of reactants. The selectivities of CO and H_2 decreased with the input power, indicating the coke formation at higher energy level, and only the ratio of CH_4/CO_2 had a significant influence on the products ratio of H_2/CO. Combining DBD plasma with g-C_3N_4 catalyst, the conversions of CH_4 and CO_2 increased and the yields of H_2 and CO were all higher than those obtained in plasma-alone system, which was attributed to the synergistic effect of plasma and g-C_3N_4 catalyst. In the DBD plasma assisted with 1% TiO_2/g-C_3N_4 composite system, the maximum conversion rate of reactants and yield of product were obtained. With further increasing the mass ratio of TiO_2, more high energy electrons could be adsorbed and thus reduced the reaction probability between high energy electrons and catalyst. The present study makes it clear that a synergy between g-C_3N_4-based catalyst and DBD plasma is achieved.

Acknowledgements This work was supported by the Joint Funds of the National Natural Science Foundation of China under Grant No. U1462105.

References

1. Chen T, Liu H, Shi P, Chen D, Song L, He H, Erost RL (2013) Fuel 107:699
2. Wilhelm DJ, Simbeck DR, Karp AD, Dickenson RL (2001) Fuel Process Technol 71:139
3. Boukha Z, Jiménez-González C, Rivas B, González-Velasco JR, Gutiérrez-Ortiz JI, López-Fonseca R (2014) Appl Catal B 158–159:190
4. Poirier MG, Trudel J, Guay D (1993) Catal Lett 21:99

5. O'Connor AM, Ross JRH (1998) Catal Today 46:203
6. Tsui M, Miyao T, Naito S (2000) Catal Lett 69:195
7. Zheng XG, Tan SY, Dong LC, Li SB, Chen HM (2015) Chem Eng J 265:147
8. Wang B, Yan W, Ge W, Duan X (2013) Chem Eng J 234:354
9. Goujard V, Tatibouet JM, Batiot-Dupeyrat C (2009) IEEE Trans Plasma Sci 37:2342
10. Wang Q, Shi HL, Yan BH, Jin Y, Cheng Y (2011) Int J Hydrogen Energy 36:8301
11. Paulussen S, Verheyde B, Tu X, Bie CD, Martens T, Petrovic D, Bogaerts A, Sels B (2010) Plasma Sources Sci Technol 19:034015
12. Wang Q, Yan BH, Jin Y, Cheng Y (2009) Plasma Chem Plasma Process 29:217
13. Paulmier T, Fulcheri L (2005) Chem Eng J 106:59
14. Eliasson B, Liu CJ, Kogelschatz U (2000) Ind Eng Chem Res 39:1221
15. Iwarere S, Rohani V, Ramjugernath D, Fabry F, Fulcheri L (2014) Chem Eng J 241:1
16. Tu X, Whitehead JC (2012) Appl Catal B 125:439
17. Gallon HJ, Tu X, Whitehead JC (2012) Plasma Process Polym 9:90
18. Pham MH, Goujard V, Tatibouet JM, Batiot-Dupeyrat C (2011) Catal Today 171:67
19. Zhou LM, Xue B, Kogelschatz U, Eliasson B (1998) Energy Fuels 12:1191
20. Kim T, Jo S, Song YH, Lee DH (2014) Appl Energy 113:1692
21. Moshrefi MM, Rashidi F, Bozorgzadeh HR, Haghighi ME (2013) Plasma Chem Plasma Process 33:453
22. Taghvaei H, Jahanmiri A, Rahimpour MR, Mohamadzadeh Shirazi M, Hooshmand N (2013) Chem Eng J 226:384
23. Lay E, Metcalfe C, Kesler O (2012) J Power Sources 218:237
24. Song HK, Lee H, Choi JW, Na B (2004) Plasma Chem Plasma Process 24:57
25. Nair SA, Nozaki T, Okazak K (2007) Chem Eng J 132:85
26. Snoeckx R, Aerts R, Tu X, Bogaerts A (2013) J Phys Chem C 117:4957
27. Vissokov GP, Panayotova MI (2002) Catal Today 72:213
28. Pietruszka B, Anklam K, Heintze M (2004) Appl Catal A Gen 261:19
29. Zheng X, Tan S, Dong L, Li S, Chen H (2014) Int J Hydrogen Energy 39:11360
30. Zhang AJ, Zhu AM, Guo J, Xu Y, Shi C (2010) Chem Eng J 156:601
31. Baylet A, Marecot P, Duprez D, Jeandel X, Lombaert X, Tatibouet JM (2012) Appl Catal B 113–114:31
32. Nozaki T, Okazaki K (2013) Catal Today 211:29
33. Cheng DG, Zhu X, Ben Y, He F, Cui L, Liu CJ (2006) Catal Today 115:205
34. Zheng X, Tan S, Dong L, Li S, Chen H (2015) J Power Sources 274:286
35. Mahammadunnisa S, Reddy PMK, Ramaraju B, Subrahmanyam C (2013) Energy Fuels 27:4441
36. Liu JL, Li XS, Zhu X, Li K, Shi C, Zhu AM (2013) Chem Eng J 234:240
37. Indarto A, Coowanitwong N, Choi JW, Lee H, Song HK (2008) Fuel Process Technol 89:214
38. Istadi NA, Amin S (2006) Fuel 85:577
39. Li Y, Xu G, Liu C, Elisson B, Xue B (2001) Energy Fuels 15:299
40. Zhang X, Dai B, Zhu A, Gong W, Liu C (2002) Catal Today 72:223
41. Wang XC, Maeda K, Thomas A, Takanabe K, Xin G, Carlsson JM, Domen K, Antonietti M (2009) Nat Mater 8:76
42. Wang XC, Blechert S, Antonietti MP (2012) ACS Catal 2:1596
43. Goettmann F, Thomas A, Antonietti M (2007) Angew Chem Int Ed 46:2717
44. Dong GH, Zhang LZ (2012) J Mater Chem 22:1160
45. Zhang J, Sun J, Maeda K, Domen K, Liu P, Antonietti M, Fu X, Wang X (2011) Energy Environ Sci 4:675
46. Ma J, Tan X, Yu T, Li XL (2016) Int J Hydrogen Energy 41:3877
47. Ma JZ, Wang CX, He H (2016) Appl Catal B 184:28
48. Boonprakob N, Wetchakun N, Phanichphant S, Waxler D, Sherrell P, Nattestad A, Chen J, Inceesungvorn B (2014) J Colloid and Interface Sci 417:4092
49. Zhang G, Zhang J, Zhang M, Wang X (2012) J Mater Chem 22:8083
50. Wang XJ, Yng WY, Li FT, Xue YB, Liu RH, Hao YJ (2013) Ind Eng Chem Res 52:1714
51. Sing KSW, Everett DH, Haul RAW (1985) Pure Appl Chem Res 57:603
52. Zhen XG, Tan SY, Dong LC, Li SB, Chen HM, Wei SA (2015) Fuel Process Technol 137:250